Supramolecular Chemistry
Publication details, including instructions for authors and subscription information:
http://www.informaworld.com/smpp/title~content=t713649759

An insight into the disorder properties of the α-cyclodextrin polyiodide inclusion complex with Sr^{2+} ion: dielectric, DSC and FT-Raman spectroscopy studies

V. G. Charalampopoulos[a]; J. C. Papaioannou[a]; K. Viras[a]; H. S. Karayianni[b]; G. Kakali[c]
[a] Laboratory of Physical Chemistry, Department of Chemistry, National and Kapodistrian University of Athens, Athens, Greece [b] Laboratory of Physical Chemistry, School of Chemical Engineering, National Technical University of Athens, Athens, Greece [c] Laboratory of Inorganic and Analytical Chemistry, School of Chemical Engineering, National Technical University of Athens, Athens, Greece

First published on: 09 June 2010

To cite this Article Charalampopoulos, V. G. , Papaioannou, J. C. , Viras, K. , Karayianni, H. S. and Kakali, G.(2010) 'An insight into the disorder properties of the α-cyclodextrin polyiodide inclusion complex with Sr^{2+} ion: dielectric, DSC and FT-Raman spectroscopy studies', Supramolecular Chemistry, 22: 9, 499 — 510, First published on: 09 June 2010 (iFirst)
To link to this Article: DOI: 10.1080/10610278.2010.487563
URL: http://dx.doi.org/10.1080/10610278.2010.487563

Supramolecular Chemistry
Vol. 22, No. 9, September 2010, 499–510

Taylor & Francis
Taylor & Francis Group

An insight into the disorder properties of the α-cyclodextrin polyiodide inclusion complex with Sr^{2+} ion: dielectric, DSC and FT-Raman spectroscopy studies

V.G. Charalampopoulos[a]*, J.C. Papaioannou[a]*, K. Viras[a], H.S. Karayianni[b] and G. Kakali[c]

[a]*Laboratory of Physical Chemistry, Department of Chemistry, National and Kapodistrian University of Athens, P.O. BOX 64004, 157 10 Zografou, Athens, Greece;* [b]*Laboratory of Physical Chemistry, School of Chemical Engineering, National Technical University of Athens, Iroon Polytechniou 9, 157 80 Zografou, Athens, Greece;* [c]*Laboratory of Inorganic and Analytical Chemistry, School of Chemical Engineering, National Technical University of Athens, Iroon Polytechniou 9, 157 80 Zografou, Athens, Greece*

(*Received 7 December 2009; final version received 18 April 2010*)

At $T < 250$ K, the polyiodide inclusion complex (α-cyclodextrin)$_2$·$Sr_{0.5}$·I_5·17H_2O displays two separate relaxation processes due to both the frozen-in proton motions in an otherwise ordered H-bonding network and the order–disorder transition of some normal H-bonds to flip-flop ones. At $T > 250$ K, the AC-conductivity is dominated by the combinational contributions of the disordered water network, the mobile Sr^{2+} ions, the polyiodide charge-transfer interactions and the dehydration process. The evolution of the Raman spectroscopic data with temperature reveals the coexistence of four discrete pentaiodide forms. In form (I) (I_3^-·I_2 ↔ I_2·I_3^-), the occupancy ratio (*x*/*y*) of the central I^- ion differs from 50/50. In form (IIa) (I_2·I^-·I_2) *x*/*y* = 50/50, whereas in its equivalent form (IIb) (I_2·I^-·I_2)* as well as in form (III) (I_3^-·I_2), *x*/*y* = 100/0 (indicative of full occupancy). Through slow cooling and heating, the inverse transformations (I) → (IIa) and (IIa) → (I) occur, respectively.

Keywords: cyclodextrin inclusion complexes; dielectric relaxation; disorder phenomena; pentaiodide transformations; Raman scattering

1. Introduction

The single crystal X-ray analysis of the polyiodide inclusion complexes of α-cyclodextrin (α-CD) with a series of metal ions (M^{n+}) (*1–3*) has revealed that they comprise systems of particular interest due to their complicated structural chemistry. More specifically, the crystalline water molecules as well as the M^{n+} ions (in most cases) act as space-fillers between the neighbouring α-CD stacks (composed of head-to-head arranged dimers) producing along with the vicinal hydroxyl groups a whole network of electrostatic and hydrogen-bonding interactions. Furthermore, the endless polyiodide chains that are embedded in the α-CD cavities consist of weakly interactive I_5^- ions; they have been not only used as models for the blue amylose–iodine complex (*2, 3*) but they have also presented remarkable electrical properties due to electron delocalisation between their I atoms.

In recent years (*4–6*), we have investigated the α-CD polyiodide complexes with Cd^{2+} and Na^+ ions (named (α-CD)-Cd and (α-CD)-Na, respectively) using a wide variety of experimental techniques that enabled valuable insights into the chemical changes as a function of temperature (120–450 K). Interestingly, dielectric spectroscopy has proven to be very sensitive to the rotational (flip-flop H-bonds (*7–9*)) and translational (H_2O molecules distributed over different sites) motion of the dipolar groups in the corresponding hydrogen-bonding networks, providing further evidence for dislocations of the metal ions and for enhanced polyiodide charge-transfer phenomena at elevated temperatures. On the other hand, FT-Raman spectroscopy has offered quite sound information about the coexistence of the different pentaiodide structural features I_2·I^-·I_2 and I_3^-·I_2 ↔ I_2·I_3^- at room temperature (which depend on the occupancy ratio *x*/*y* of the central I^- anion and are analytically described in Figure 1(a)) and their impressive interconversions (exhibited in Figure 1(b)–(d)) during the cooling and heating of the crystals. Finally, differential scanning calorimetry (DSC) and simultaneous thermal analysis (STA) effectively detected both the gradual removal (dehydration process) of the interstitial water molecules with various energy contents and the degradation of polyiodide moieties due to the sublimation of iodine.

These findings explicitly indicate that the aforementioned inclusion complexes are excellent models for the elucidation of principal forces, dynamic properties and charge transport mechanisms in the water clusters of biological systems (*10–14*), in the building blocks of many polyiodide materials (*15*) and in the cyclodextrin complex formation processes (*16*, *17*). Despite the fact that the individual nature of each counterion appears to have a

*Corresponding authors. Emails: jpapaioannou@chem.uoa.gr; v_charalampopoulos@yahoo.gr

ISSN 1061-0278 print/ISSN 1029-0478 online

DOI: 10.1080/10610278.2010.487563
http://www.informaworld.com

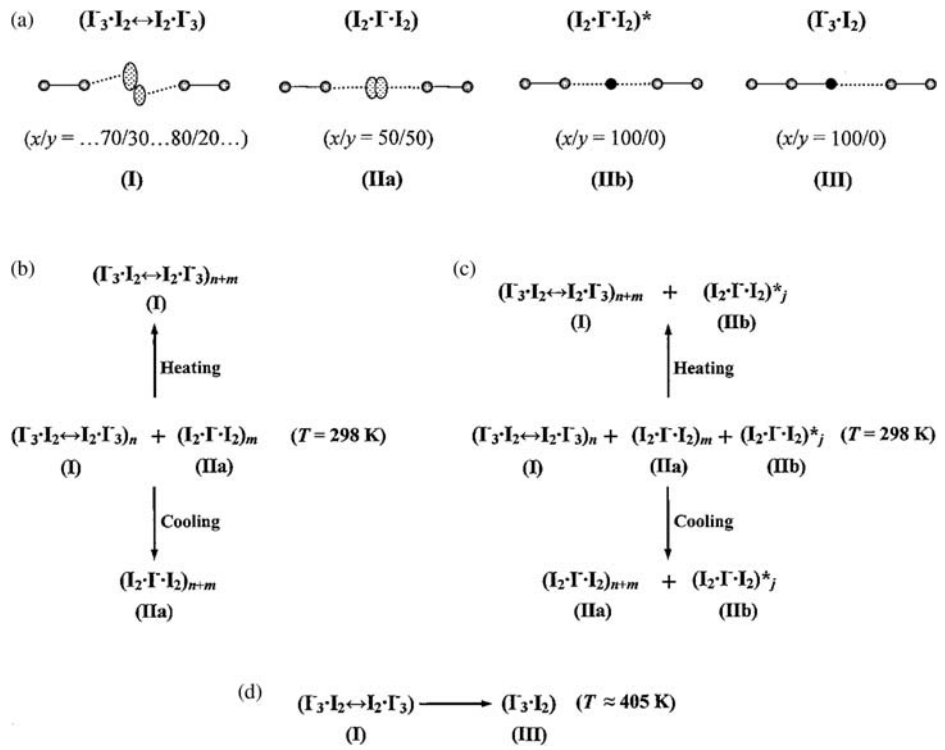

Figure 1. The four discrete pentaiodide forms that have been detected in $(\alpha\text{-CD})_2\cdot Cd_{0.5}\cdot I_5\cdot 26H_2O$ ((α-CD)-Cd) and $(\alpha\text{-CD})_2\cdot NaI_5\cdot 8H_2O$ ((α-CD)-Na) (*5,6*): (a) In form (I), the occupancy ratio *x/y* of the disordered central I^- ion is different from 50/50 (e.g. …70/30…80/20…). In form (IIa), the occupancy ratio of the I^- ion is 50/50. In form (IIb), the I^- ion is well ordered and equidistant from the two I_2 units. The value of 100/0 does not have any physical sense and is used to illustrate full occupancy. In form (III), the central I^- anion is well ordered forming with the one of the two I_2 units an I_3^- ion. (b) In (α-CD)-Cd, the transformation (I) → (IIa) takes place during cooling, whereas the inverse one (IIa) → (I) happens during heating. (c) (α-CD)-Na displayed similar behaviour to the one of (α-CD)-Cd further presenting the form (IIb) which remained unaffected by temperature. (d) At ~ 405 K, both systems exhibit the disorder–order transition (I) → (III) via a charge-transfer interaction between the I^- ion and one of the two I_2 units.

strong influence on the resultant crystalline form (*1–3*), it also appears to affect in a unique manner (along with slight variations in experimental conditions during synthesis and crystallisation) the following: (i) the extent of the relevant disorder phenomena in the corresponding hydrogen bonding networks (*4–6*) and (ii) the obtained configuration of the solid polyiodide structures (*15*, *18*). Thus, in the present contribution we expand our experimental studies to one more α-CD polyiodide inclusion complex with Sr^{2+} ion (named (α-CD)-Sr) relying on the combinational application of dielectric relaxation, FT-Raman spectroscopy and thermal analysis. Our main aim is not only a thorough interpretation of the respective physicochemical properties (dipolar orientational correlations, polyiodide structural conversions, electron interactions and thermal dissociations) but also a valid corroboration of our preliminary conclusions.

2. Experimental

α-CD and solid iodine were obtained from Fluka Chemica whereas strontium iodide (SrI_2) was obtained from Alfa Aesar. α-CD, 5.50 g, (5.66 mmol) was dissolved in distilled water (40 mL) at room temperature under continuous stirring (full dissolution). Then, 0.195 g of strontium iodide (0.571 mmol) and 0.22 g of solid iodine (0.866 mmol) were simultaneously added to the solution which was heated up to 70°C for 20–25 min. The hot solution was quickly filtered through a folded filter paper into an empty beaker (100 mL) which was covered with Teflon and then immersed in a Dewar flask (500 mL) containing water at the same temperature. After two days, very fine thin needles of (α-CD)-Sr were grown with golden lustre and uniform composition. These were isolated by filtration and dried in air.

Simultaneous thermogravimetry analysis (TGA) and differential thermal analysis (DTA) of the crystals were conducted using a NETZSCH-STA 409 EP Controller TASC 414/3 (reference Al_2O_3). The sample (65.90 mg) was heated in the temperature range of 20–135°C with a heating rate of 5°C min^{-1}. The C content of (α-CD)-Sr was determined microanalytically on a LECO CS 230 analyser (combustion analysis), whereas the Sr content was measured on a Perkin-Elmer Optima 5300 DV

ICP-OES (inductively coupled plasma-optical emission spectrometer).

The experimental X-ray powder diffraction pattern was obtained with a Siemens D 5000 diffractometer using CuKa1 radiation ($\lambda = 1.54059$ Å) at 40 kV, 30 mA and a graphite crystal monochromator. The diffraction data were collected in the 2θ range of 5–55° with a constant step of 0.015° and a dwell time of 7s/step. The calculation of the simulated X-ray powder diffraction pattern of $(\alpha\text{-CD})_2 \cdot Cd_{0.5} \cdot I_5 \cdot 27H_2O$ (*2*, *3*) and the Rietveld refinement of the lattice parameters were performed by the computer program POWDERCELL 2.4 developed by Nolze and Kraus (*19–23*).

The differential scanning calorimetry method (Perkin-Elmer DSC-4 instrument) was applied using a thermal analysis data station (TADS) system for all calorimetric measurements. Known weights (10–15 mg) of (α-CD)-Sr were sealed into aluminium pans and then heated from 0 up to 170°C with a heating rate of 10°C min^{-1}, under a dynamic nitrogen atmosphere. The instrument was calibrated using indium at the same scanning rates.

For the dielectric spectroscopy experiment, a pressed pellet of powdered sample (542.5 mg), 20 mm in diameter with thickness 1.05 mm, was prepared with a pressure pump (Riken Powder model P-1B) at room temperature. Two platinum foil electrodes were pressed at the same time with the sample. The electrical measurements were taken using a low-frequency (0–100 kHz) dynamical signal analyser (DSA-Hewlett-Packard 3561A) at the temperature range of 110–440 K. The data can be transferred to a PC through an HP 82335 Interface Bus (IEEE-488), where they can be stored and analysed by a software program (*2plt*-1996). The complex permittivity ε^*, impedance Z^*, conductivity σ^* along with the phase shift φ and the respective Argand diagrams (ε'' vs. ε' and Z'' vs. Z') can be calculated and plotted as a function of both temperature and applied frequency. An analytical description of the process is given in previous studies (*24*, *25*).

The Raman spectra were obtained at 4 cm^{-1} resolution from 3500 to 100 cm^{-1} with a data point interval of 1 cm^{-1} using a Perkin-Elmer NIR FT-spectrometer (Spectrum GX II) equipped with an InGaAs detector. The laser power and spot (Nd: YAG at 1064 nm) were controlled to be constant at 50 mW during the measurements and 400 scans were accumulated. Two experiments were performed in the temperature ranges of (a) (−130) − 25°C (cooling) and (b) 30–130°C (heating), with different samples. During the cooling process, the sample was enclosed in a glassy NMR tube and held at a constant temperature (±1°C) by means of a low temperature cell (Ventacon, Winchester, UK). The temperature variation was controlled with a Ventacon Winchester instrument equipped with a CALCOMMS 3300 autotune controller.

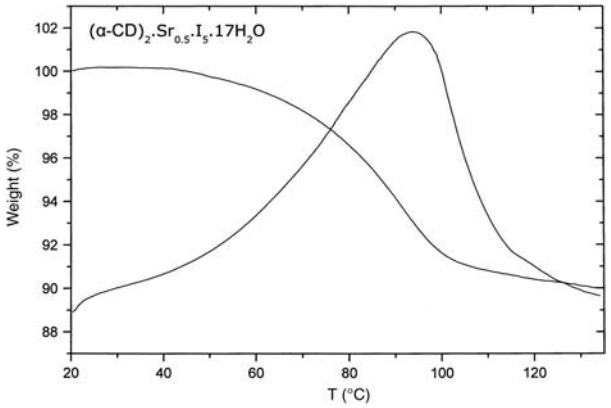

Figure 2. Simultaneous TGA and DTA of $(\alpha\text{-CD})_2 \cdot Sr_{0.5} \cdot I_5 \cdot 17H_2O$, with a heating rate of 5°C min^{-1}.

3. Results and discussion

3.1 Characterisation of the synthesised inclusion complex

The TGA and DTA curves of (α-CD)-Sr from room temperature to 135°C (heating rate: 5°C min^{-1}) are shown in Figure 2. The number of water molecules per dimer was calculated from the weight loss (10.10%) in the temperature range of ~ 46–133°C, where the dehydration process gradually takes place. The result is in agreement with ~ 17 water molecules per α-CD dimer. Furthermore, we have carried out the %C and %Sr elemental analysis of (α-CD)-Sr in order to achieve a more complete determination of its general composition, and this is explained in the following discussion. It has been shown that the α-CD polyiodide inclusion complexes with metal ions display at least four different crystalline forms that strongly depend on the nature of the counterion and its coordination scheme (*1–3*). Among other cations, cadmium and strontium ions were classified into those which induce a tetragonal crystalline form with space group $P4_22_12$. Taking into account the fact that the single crystal X-ray analysis of (α-CD)-Cd at room temperature (*2*, *3*) revealed that cadmium ions were twofold disordered with 0.5 Cd^{2+} per α-CD dimer (general composition $(\alpha\text{-CD})_2 \cdot Cd_{0.5} \cdot I_5 \cdot 27H_2O$), in the present case the elucidation of the statistical distribution of Sr^{2+} ions in relation to the α-CD dimers appears to be crucial. The elemental analysis provided the following data: C, 29.86% and Sr, 1.63%. The corresponding %C, %Sr calculated values are 29.51 and 1.49% for 0.5 Sr^{2+} per dimer (Sr to C ratio 1:19.80) and 29.08 and 2.95% for 1.0 Sr^{2+} per dimer (Sr to C ratio 1:9.86). It becomes apparent that the obtained experimental values as well as the experimental Sr to C ratio (1:18.32) approach the respective calculated ones for a twofold disordered strontium ion (0.5 Sr^{2+} per dimer), indicating that the general composition of (α-CD)-Sr can be described as $(\alpha\text{-CD})_2 \cdot Sr_{0.5} \cdot I_5 \cdot 17H_2O$.

For the X-ray powder diffraction method (XRPD), a few grams of needle-shaped (α-CD)-Sr crystals were finely hand-pulverised aiming at reducing the greater volume fraction of certain crystal orientations (texture) in the powdered sample. The experimental XRPD pattern was collected at room temperature covering the 5–55° 2θ range, in order to carry out a Rietveld refinement of the lattice parameters. Figure 3 shows the experimental XRPD pattern of (α-CD)-Sr and the Rietveld refinement of this profile (POWDER CELL 2.4 software) with the tetragonal $P4_22_12$ structure of $(\alpha\text{-CD})_2\cdot Cd_{0.5}\cdot I_5\cdot 27H_2O$ (*2*,*3*): $R_p = 10.17\%$, $R_{wp} = 16.28\%$, $R_{exp} = 10.96\%$ and $\chi^2 = 2.206$. We obtained the following lattice parameters $a = b = 19.9281(5)$Å and $c = 30.8151(7)$Å which are in very good agreement with the unit cell constants reported by Noltemeyer and Saenger (*2*, *3*). At this point, we clarify that some experimental reflection intensities vary from the corresponding ones of the simulated XRPD pattern due to the following reasons: (i) most of the pentaiodide units in (α-CD)-Sr display different configurations from those described in the single crystal of (α-CD)-Cd as it becomes evident from the FT-Raman spectroscopy study, (ii) in (α-CD)-Sr, the degree of hydration per dimer (17 H_2O) is lower than that of (α-CD)-Cd (27 H_2O), indicating that the crystalline water molecules of these systems are neither expected to occupy equivalent lattice positions nor to present identical spatial correlations and (iii) an inevitable though little contribution of preferred orientation effects. Nevertheless, the observed isomorphism between (α-CD)-Sr and (α-CD)-Cd reveals that the α-CD molecules of the former are arranged coaxially with the crystallographic *c* axis (Figure 4), exhibiting a rotation to each other by 13° as in the case of the latter complex (*2*, *3*). This structural feature is consistent with the formation of wide enough interstices between the α-CD stacks. These interstices accommodate 17 water molecules per α-CD dimer along with the twofold disordered Sr^{2+} ions (*2*). Finally, the total absence of any hump (indicative of amorphous material) in the experimental XRPD pattern proves the purity of the synthesised inclusion complex (single-phase compound).

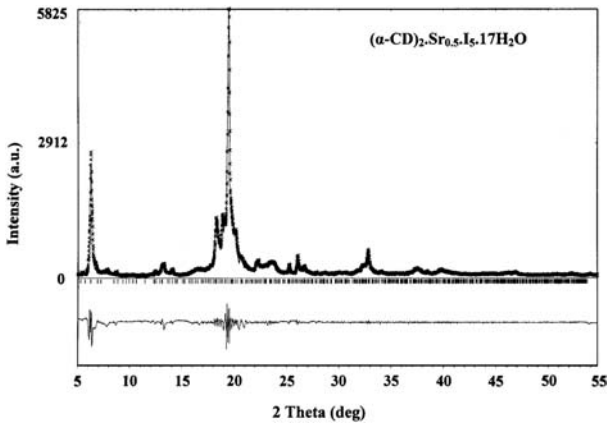

Figure 3. Rietveld refinement pattern of $(\alpha\text{-CD})_2\cdot Sr_{0.5}\cdot I_5\cdot 17H_2O$. Black crosses, experimental pattern; solid line, refined model. The curve at the bottom is the difference between the observed and calculated intensities in the same scale. Black vertical lines indicate the positions of the allowed reflections.

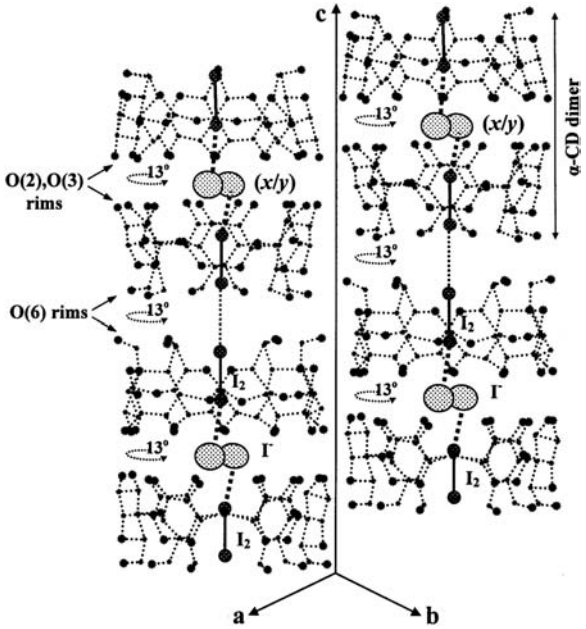

Figure 4. The crystalline structure of $(\alpha\text{-CD})_2\cdot Sr_{0.5}\cdot I_5\cdot 17H_2O$ based on the single crystal X-ray crystallography analysis of the isomorphous $(\alpha\text{-CD})_2\cdot Cd_{0.5}\cdot I_5\cdot 27H_2O$ (tetragonal $P4_22_12$), carried out by Noltemeyer and Saenger (*2*,*3*).The α-CD stacks are strictly linear and arranged coaxially with the crystallographic c axis, leaving large spaces between them. The disordered I^- anions are presented as spotted ellipsoids, whereas the well-ordered I atoms are presented as small spotted spheres.

3.2 Disorder in polyiodide moieties

A preliminary comparison of the present FT-Raman spectroscopy results to those obtained from our previous investigations (*5*, *6*) reveals that (α-CD)-Sr displays a rather similar behaviour to that of (α-CD)-Na (Figure 1(c)) during the cooling and heating processes. More specifically, at room temperature (25°C) there is a strong band at 156 cm^{-1} (Figure 5(a)) which is ascribed to the symmetric coupling of the v_1 stretching vibration of the outer I—I bonds in a $(I_2\cdot I^-\cdot I_2)$ configuration (form (IIa) according to Figure 1(a)), and an easily distinguished shoulder at 169 cm^{-1} which is attributed to the v_1' symmetric vibrational mode of a weakly coordinated I_2 unit in a $(I_3^-\cdot I_2 \leftrightarrow I_2\cdot I_3^-)$ configuration (form (I) according to Figure 1(a)) (*15*, *18*, *26–32*). As the temperature is lowered to −130°C (Figures 5(a),(b)), the band at 156 cm^{-1} is slightly shifted to the higher frequency of 158 cm^{-1} and presents an intensity enhancement in

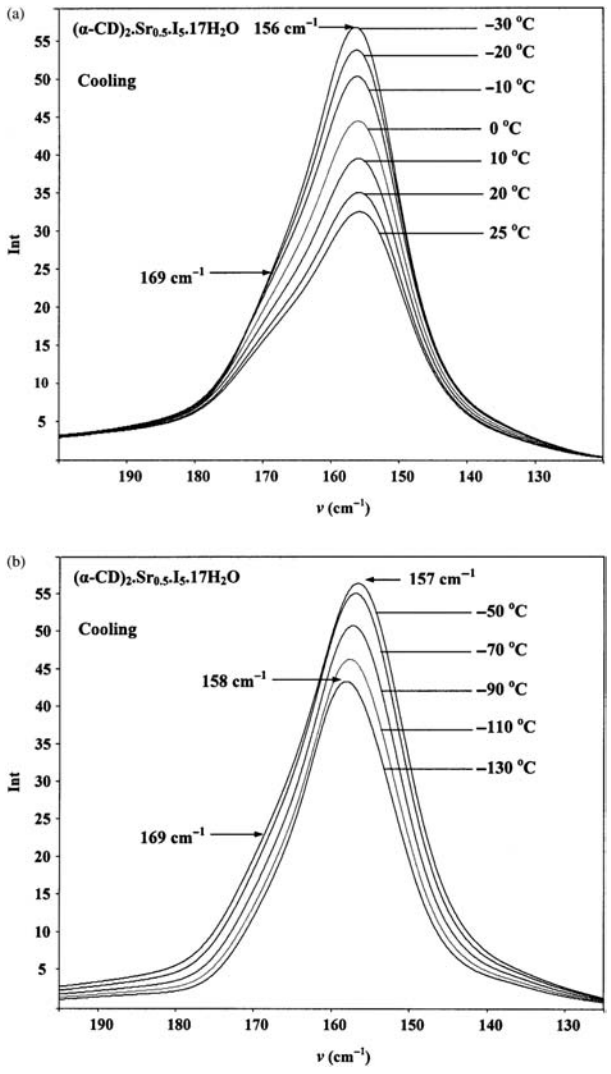

Figure 5. Raman spectra of $(\alpha\text{-CD})_2{\cdot}Sr_{0.5}{\cdot}I_5{\cdot}17H_2O$ during cooling, in the temperature ranges of (a) (−30)–25°C and (b) (−130)–(−50)°C.

relation to the shoulder at 169 cm^{-1}, which becomes so weak that it is barely identifiable. These experimental data are consistent with the pentaiodide structural transformation (I) → (IIa) which is a consequence of the fact that the occupancy ratio of the disordered I^- ions in form (I) gradually changes from an initial value of, for example, ...60/40...70/30... to the final value of 50/50 (form (IIa)) as the crystals are slowly cooled. Figure 6 exhibits the variation of the intensity ratio I_{169}/I_{156} as a function of temperature. From 25 to −110°C, this ratio decreases due to the continuous transformation (I) → (IIa). In the range of (−130)–(−110)°C, it remains almost invariant indicating that the aforementioned transformation is completed and that there is a very small population of $(I_3^-{\cdot}I_2)$ ions (form (III) according to Figure 1(a)) that does not display any configurational conversion with

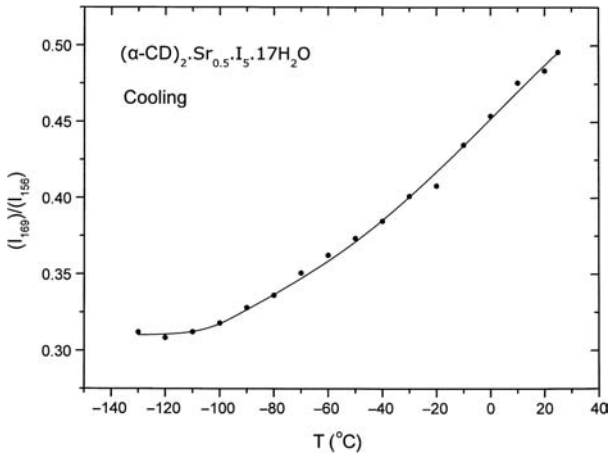

Figure 6. The temperature dependence of the Raman intensity ratio $(I_{169})/(I_{156})$ of $(\alpha\text{-CD})_2{\cdot}Sr_{0.5}{\cdot}I_5{\cdot}17H_2O$ during the cooling process.

temperature, retaining the hardly distinguished shoulder at 169 cm^{-1}.

Complementary information is provided by the FT-Raman spectra of (α-CD)-Sr in the temperature range of 30–130°C (Figure 7(a)–(c)). Initially, there is a strong band at 156 cm^{-1} and an easily distinguished shoulder at 169 cm^{-1}. As the temperature is raised, the band at 169 cm^{-1} becomes more intense in comparison to that at 156 cm^{-1} and accompanying this relative intensity change there is also a small position shift of the former band to the frequency of 171 cm^{-1} and of the latter band to the frequency of 161 cm^{-1}. These phenomena are caused by the transformation (IIa) → (I) which implies a progressive change of the occupancy ratio of the I^- ions in the initial (25°C) form (IIa), from 50/50 to the value of ...60/40...70/30... and so on. Similar changes also happen to the occupancy ratio of the I^- anions in the initial (25°C) form (I) (e.g. ...60/40...70/30... → ...70/30...80/20...). Thus, it appears to be explicit that as the temperature increases, the vario-occupancy ratio of the disordered ions I^- in the pentaiodide forms (I) and (IIa) presents the tendency to take the value of 100/0 (indicative of full occupancy). The disordered I^- ions in form (I) will become well ordered earlier than those in form (IIa), according to the disorder–order transition (I) → (III) (Figure 1(d)). This effect takes place via a charge-transfer interaction (as evident from dielectric measurements) between the central I^- ion (Lewis base donor) and one of the two I_2 molecules (Lewis acid acceptors). The fact that the shoulder at 161 cm^{-1} is retained up to the end of the experiment suggests that there is an important per cent of pentaiodide ions which is described by the $(I_2{\cdot}I^-{\cdot}I_2)^*$ configuration (form (IIb) according to Figure 1(a)) and remains unaffected during the slow heating of the sample. Figure 8 shows that the temperature-dependent intensity ratio I_{169}/I_{156} continuously increases from 30 to 100°C due to the gradual transformation

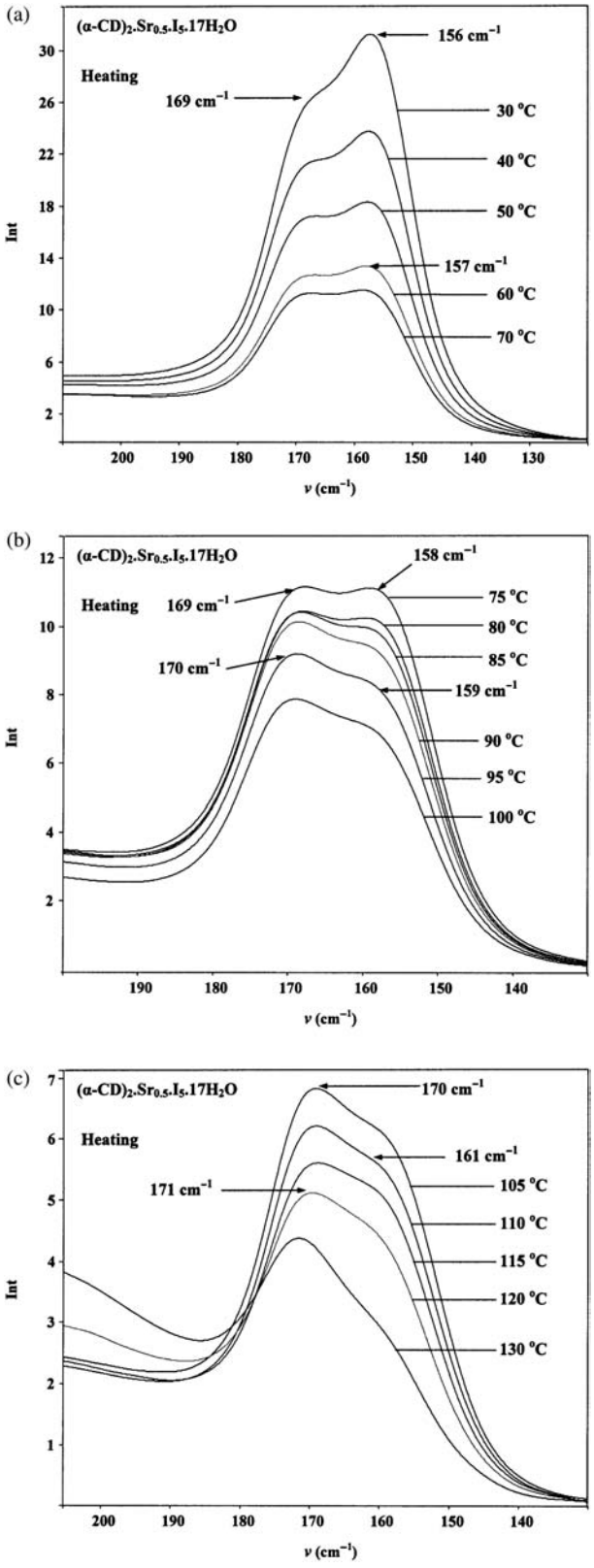

Figure 7. Raman spectra of $(\alpha\text{-CD})_2{\cdot}Sr_{0.5}{\cdot}I_5{\cdot}17H_2O$ during heating, in the temperature ranges of (a) 30–70°C, (b) 75–100°C and (c) 105–130°C.

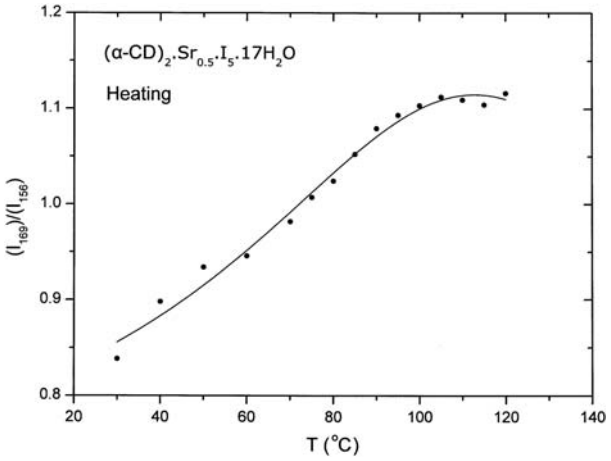

Figure 8. The temperature dependence of the Raman intensity ratio $(I_{169})/(I_{156})$ of $(\alpha\text{-CD})_2{\cdot}Sr_{0.5}{\cdot}I_5{\cdot}17H_2O$ during the heating process.

(IIa) → (I). Above 100°C, this ratio remains almost constant revealing that all the $(I_2{\cdot}I^-{\cdot}I_2)$ ions of form (IIa) have been transformed into those of form (I), whereas the $(I_2{\cdot}I^-{\cdot}I_2)^*$ ions of form (IIb) still exist in the crystal lattice. The initial very small population of $(I_3^-{\cdot}I_2)$ ions (form (III)) which has been detected during cooling is also expected to present no configurational conversions with temperature rise.

The characteristic Raman-active (symmetric stretch) band v_1'' of the I_3^- ions at approximately $107\,cm^{-1}$ (*27*, *28*, *33*) does not appear as a result of the limited frequency range of the spectrometer ($\geq 100\,cm^{-1}$). Nevertheless, in Figure 9(a) and (b), we observe its progressive overtones at 211 ($2v_1''$, 2×107) and $307\,cm^{-1}$ ($3v_1''$, 3×107), whose intensity variation obviously follows the intensity variation of the band at $169\,cm^{-1}$ (v_1') as a function of temperature in both cooling (up to the final temperature of −130°C) and heating (up to the selected temperature of 110°C) processes. This spectral behaviour as well as the existence of the combination band at $276\,cm^{-1}$ ($v_1'' + v_1'$, $107 + 169$) comprises further assurances that the v_1'' and v_1' fundamental transitions originate from a single chemical species ($I_3^-{\cdot}I_2$, $I_3^-{\cdot}I_2 \leftrightarrow I_2{\cdot}I_3^-$). Interestingly, at the high temperature of 130°C (Figure 9(b)), additional information is drawn allowing a probe into both the local and long-range order fluctuations of the polyiodide moieties. More specifically, as it can be observed, the broadened $3v_1''$ band exhibits a downshift to the frequency of $299\,cm^{-1}$, indicating a downshift of the non-detectable parent fundamental band v_1'' at $\sim 107\,cm^{-1}$. This phenomenon is attributed to the initiation of the sublimation of iodine which is directly related to the band at $214\,cm^{-1}$ (characteristic of the sublimating I_2) (*15*) and results in the breaking of the

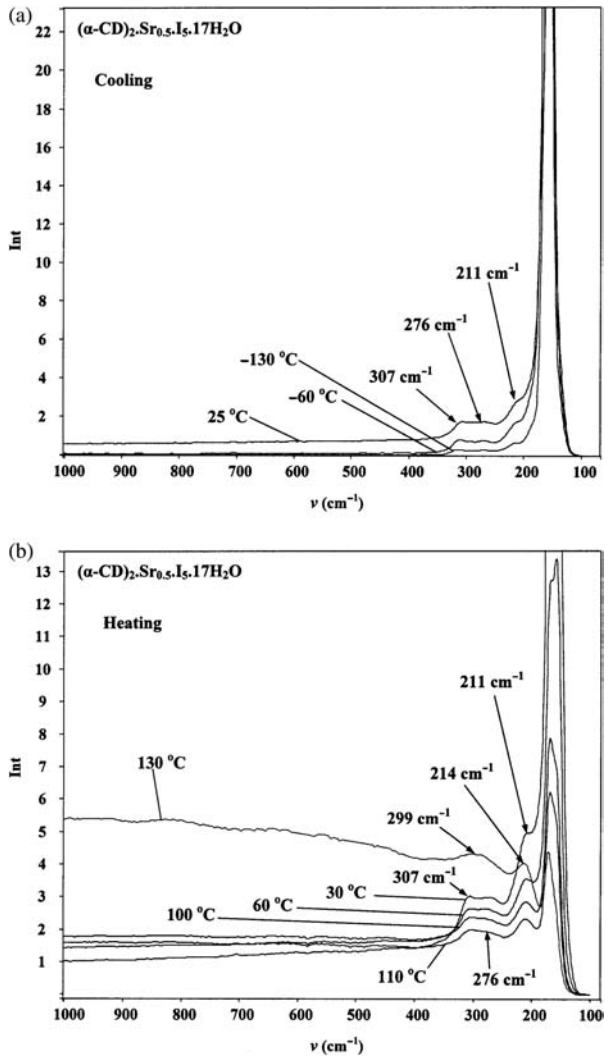

Figure 9. Raman spectra of $(\alpha\text{-CD})_2{\cdot}Sr_{0.5}{\cdot}I_5{\cdot}17H_2O$ in the extended frequency range of 100–1000 cm^{-1} (a) at the representative temperatures of 25, −60 and −130°C during cooling and (b) at the representative temperatures of 30, 60, 100, 110 and 130°C during heating.

$(I_3^-{\cdot}I_2)$, $(I_3^-{\cdot}I_2 \leftrightarrow I_2{\cdot}I_3^-)$ and $(I_2{\cdot}I^-{\cdot}I_2)$* chain compounds into I_3^- and I_2 (*26*, *31*, *34*). This process increases both the I_3^- chain population and the I_2 sublimating population at the expense of pentaiodide units, explaining the enhanced intensities of the $3v_1''$ and 214 cm^{-1} bands in relation to those of the bands at 161 (v_1) and 171 cm^{-1} (v_1'). Moreover, we strongly believe that the shift of the v_1'' and $3v_1''$ vibrational modes of I_3^- ions to lower frequencies is a result of both the emerging $I_3^-{\cdots}I_3^-$ excitonic interactions along the chain length (head-to-tail arrangement of transition dipole moments) and the I_3^- thermal tension (*34*, *35*). The latter phenomenon may also play a key role in the observed broadening of the $3v_1''$ band. Concerning the combination band $(v_1'' + v_1')$, it weakens and becomes obscured by the $3v_1''$ band as a result of the important reduction of $(I_3^-{\cdot}I_2)$ and $(I_3^-{\cdot}I_2 \leftrightarrow I_2{\cdot}I_3^-)$ units due to the sublimation of iodine. Finally, the band at 214 cm^{-1} seems to obscure the $2v_1''$ overtone which is also expected to present a frequency downshift and make an essential contribution to the intensity of the former band. At this point, the fact that at even higher temperatures the total degradation of the polyiodide chains takes place is also emphasised.

In summary, the present work, via the temperature-dependent FT-Raman spectroscopy, sheds light on the relatively unknown mechanisms of ion transport at the atomic scale by detecting a series of detailed snapshots of the disordered I^- ions during the underlying pentaiodide interconversions. Within this perspective, this system could be used as a model for the elucidation of the charge-transfer processes in a variety of biological materials that display a vario-degree of ion disorder under different experimental conditions. Apart from the above findings, the employment of Raman technique also reveals that the endless polyiodide chains of (α-CD)-Sr consist of four discrete pentaiodide substructures at room temperature. This should not appear unfamiliar to the reader because it is widely shared among chemists that the real crystals present deviations from the ideal picture of a periodical perfect repetition of a unit cell (*36*). Even though we have credibly demonstrated that the occupancy ratio (*x*/*y*) of the disordered central I^- ions seems to be exclusively responsible for the predominant pentaiodide form during the thermal variation of the sample, it is clear that some significant questions remain concerning the nature of this disorder. A detailed crystallographic study over a range of temperatures by a specialist can effectively determine the evolution of the atomic displacement parameters in order to achieve a successful discrimination between dynamic, static and thermal vibrational disorders (*36–39*). Although, a discussion of this particular topic is beyond the scope of the present work, we believe that dynamic phenomena make a fundamental contribution to the temperature-dependent distribution of the electronic density of I^- ions. In such a case, the lifetime of the ground state of the interconverting pentaiodide species is expected to be longer than that of the Raman vibrational scale (10^{-13} sec) (*40*). Furthermore, it is worth stressing that the small position shifts of the two initial bands (156 and 169 cm^{-1}) to higher wavenumbers during cooling (156 → 158 cm^{-1}) and heating (156 → 161 cm^{-1} and 169 → 171 cm^{-1}) may arise from small geometrical transformations involving not only slight decrements in the I_2 bond lengths (attenuation of donor–acceptor interactions, increased I_2 force constant) (*15*, *41*) but changes in the bond angles of the pentaiodides as well. According to the *ab initio* calculations of Sharp and Gellene (*42*), the highly bent (C_{2v} symmetry) and the linear ($D_{\infty h}$ symmetry) $I_2{\cdot}I^-{\cdot}I_2$ ions present a symmetric stretch of the outer I—I bonds at 157.4 and 165 cm^{-1},

respectively. Additionally, both the resonance Raman spectroscopy studies of starch–iodine samples by Teitelbaum et al. (*26*) and of (α-CD)-Cd and (α-CD)-Li single crystals by Mizuno et al. (*28*) have shown that the linear $I_2{\cdot}I^-{\cdot}I_2$ chain compounds exhibit the aforementioned vibrational mode in the narrow range of 161–163 cm^{-1}. Taking into consideration these results, the shift of the band at 156 cm^{-1} to the frequency of 161 cm^{-1} with temperature rise (Figures 8(a)–(c)) can be interpreted in terms of a gradual conversion of a C_{2v} point group symmetry to a $D_{\infty h}$ one.

3.3 Thermal stability

The DSC trace of (α-CD)-Sr recorded with a scan rate of 10°C·min^{-1} is shown in Figure 10. The strong endothermic peak at 109°C and the easily distinguished shoulder at 123°C are directly related to the removal of the two kinds of water molecules which coexist in the crystal lattice. More specifically, the former peak corresponds to the gradual evaporation of the water molecules with a higher energy content than those whose evaporation is responsible for the latter peak. This discrimination can be explained by taking into account the differences traced in the local environments of the water molecules. At room temperature, some of them are neatly coordinated (tightly bound state) with fully occupied positions, whereas others are positionally disordered (easily movable state), exhibiting extensive thermal motions and less favourable hydrogen bond geometries (*3*, *7–9*, *43*). Through the slow heating of the crystals, the relative populations of the two kinds of water molecules change inversely as a function of temperature (the disordered H_2O molecules increase whereas the well-ordered ones decrease). During the dehydration process, the loss of the disordered water molecules is expected to take place at lower temperatures than the loss of the well-ordered water molecules. The strong peak at 109°C is consistent with an enthalpy change

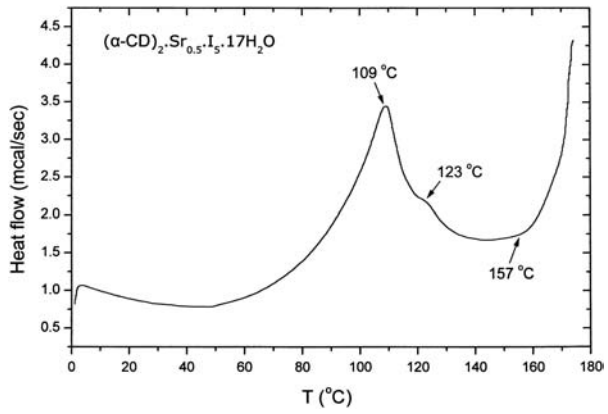

Figure 10. DSC thermogram of $(\alpha\text{-CD})_2{\cdot}Sr_{0.5}{\cdot}I_5{\cdot}17H_2O$ with a heating rate of 10°C/min.

ΔH which is greater than the one in the case of the shoulder at 123°C, revealing that as the temperature is being raised there is an enormous increment of the disorder in the interstitial water arrangement and only a small per cent of H_2O dipoles remains in the tightly bound state.

The upward baseline at $T > 157$°C is interpreted in terms of the sublimation of iodine which involves the gradual degradation of the I_5^- ions and the subsequent effusion of the sublimed iodine molecules, resulting in the rupture of the grain boundaries. This process should not be related to the decomposition of the α-CD molecules because the latter begins at temperatures higher than 250°C (*44*). In our previous studies, we examined a series of β-CD polyiodide complexes with various metal ions (*25*, *45–47*) and we found that the sublimation of iodine took place at lower temperatures (130–135°C) than in the present case. This happens because (i) the neighbouring I_5^- ions in (α-CD)-Sr are weakly interactive (electron delocalisation), whereas the neighbouring I_7^- ions in the β-CD systems are non-interactive and (ii) the α-CD cavities are narrower than those of β-CDs indicating much more stronger C—H···I dispersion forces (*3*).

3.4 Disorder in the hydrogen-bonding network

Dielectric relaxation spectroscopy (DRS) is a powerful method for the detection of all the electrical conduction mechanisms within a whole series of materials. In the present case, the data were analysed in terms of the complex permittivity ε^*, the complex impedance Z^*, the phase shift φ (or phase angle) and the complex conductivity σ^*. Complex permittivity ε^* is defined as follows (*48–50*):

$$\varepsilon^*(f) = \varepsilon'(f) - j\varepsilon''(f), \tag{1}$$

where the real part ε' is directly related to the variations of the total polarisation, the imaginary part ε'' (loss factor) expresses the energy dissipation within the sample, f is the frequency of the applied electric field and $j = \sqrt{-1}$. Complex impedance Z^* is described by the following relation:

$$Z^*(f) = Z'(f) - jZ''(f). \tag{2}$$

Generally, the complex plane plots, imaginary Z'' vs. real Z', are used in order to gain valuable information about the relaxation processes that take place in the systems under investigation. In the rare case of a single relaxation time τ, a perfect semicircle is formed (Debye relaxation) whose diameter corresponds to the resistance of the material and its centre is localised on the real axis. When there is a distribution of relaxation times, a semicircular arc appears (Cole–Cole relaxation) having its centre lying below the real axis. The complex impedance Z^* and the

complex permittivity ε^* are interrelated as (*50*)

$$\varepsilon^*(f) = \frac{1}{j\omega C_o Z^*(f)}, \quad (3)$$

where $\omega = 2\pi f$ is the angular frequency, $C_o = \varepsilon_o A_c/l$ is the capacitance of the empty measuring cell of electrode area A_c and electrode separation length l. The quantity ε_o is the dielectric permittivity of free space ($8.854 \cdot 10^{-12}$ F/m).

The phase difference φ (also known as phase shift or phase angle) between the applied voltage $V^*(t)$ and the resulting current $I^*(t)$ is given by the relation (*50*)

$$\varphi = \tan^{-1}\left(\frac{Z''(f)}{Z'(f)}\right), \quad (4)$$

while the complex conductivity σ^* is represented by the following expression (*49*):

$$\sigma^*(f) = \sigma'(f) + j\sigma''(f), \quad (5)$$

being related to the complex permittivity ε^* and the complex impedance Z^* as (*49*, *50*)

$$\sigma^*(f) = j\omega\varepsilon_o\varepsilon^*(f) = \frac{1}{Z^*(f)}. \quad (6)$$

Concerning the polycrystalline (α-CD)-Sr, DRS reveals that at low temperatures this system presents a different dielectric behaviour from that of the previously investigated (α-CD)-Cd and (α-CD)-Na complexes (*4*–*6*). More specifically, in the temperature range of 110–250 K, what becomes obvious is the presence of two sigmoid curves in the $\varepsilon'(T)$ variation (inflection points $\varepsilon' = 7.8$ at $T = 128.8$ K and $\varepsilon' = 15.5$ at $T = 173.7$ K, Figure 11), of two loss peaks in the $\varepsilon''(T)$ variation ($\varepsilon''_{1\max} = 0.9$ at $T = 128.8$ K and $\varepsilon''_{2\max} = 2.7$ at $T = 173.7$ K, Figure 12) and of two topical minima in

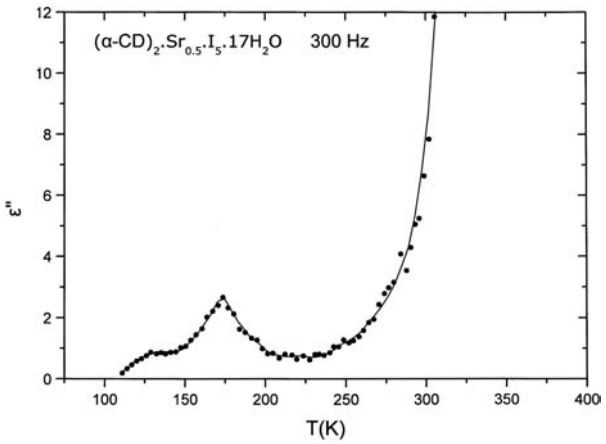

Figure 12. Temperature dependence of the imaginary part ε'' of the dielectric constant of $(\alpha\text{-CD})_2\cdot Sr_{0.5}\cdot I_5\cdot 17H_2O$ at 300 Hz.

the $\varphi(T)$ variation ($\varphi_{1\min} = 83.6^\circ$ at $T = 128.8$ K and $\varphi_{2\min} = 80.2^\circ$ at $T = 173.7$ K, Figure 13). These experimental data indicate two separate relaxation processes which result in important changes in the sample polarisation and are directly related to the motions of the water molecules and the hydroxyl groups in the crystal lattice. The transition temperature $T_{\text{trans}} = 173.7$ K is consistent with the order–disorder transition of some normal hydrogen bonds to those of flip-flop type according to the following scheme:

$$\underset{\text{normal H-bonds}}{\text{O—H}\cdots\text{O—H}} \quad \rightarrow \quad \underset{\text{flip-flop H-bonds}}{\text{O—(1/2H)}\cdots\text{(1/2H)—O}}. \quad (7)$$

Flip-flop hydrogen bonds are characterised by the existence of H-atoms that are dynamically disordered in two energetically near equivalent positions (entropically favoured). This type of H-bonds has been originally

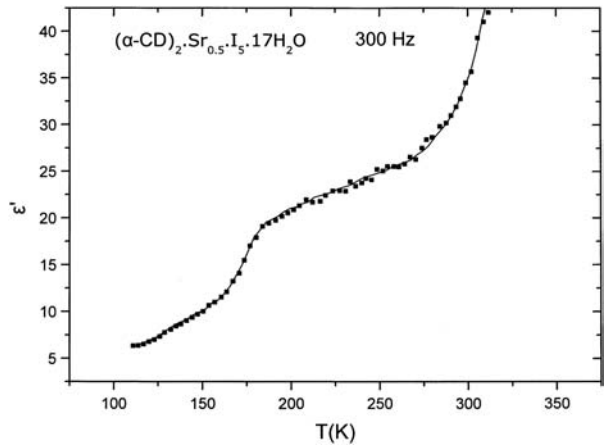

Figure 11. Temperature dependence of the real part ε' of the dielectric constant of $(\alpha\text{-CD})_2\cdot Sr_{0.5}\cdot I_5\cdot 17H_2O$ at 300 Hz.

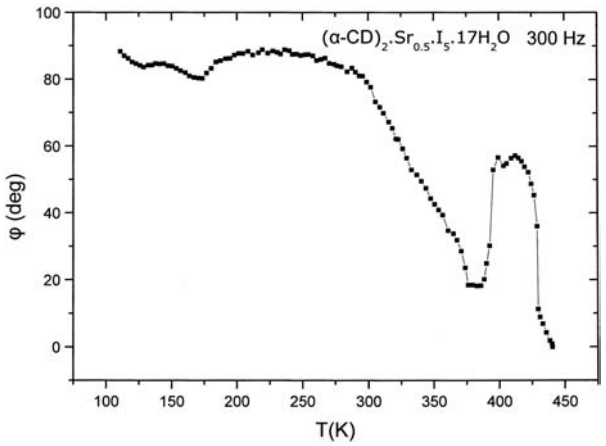

Figure 13. Temperature dependence of the phase shift φ of $(\alpha\text{-CD})_2\cdot Sr_{0.5}\cdot I_5\cdot 17H_2O$ at 300 Hz.

detected in the single crystal of β-CD·11H_2O at room temperature by means of neutron diffraction analysis carried out by Betzel et al. (*8*).

The relaxation peak at 128.8 K (Figure 12) can be interpreted in terms of a frozen-in disorder which is associated with the persistence of a certain per cent of molecular motions in the hydrogen-bonding network of (α-CD)-Sr. Such a behaviour can be explained by taking into consideration the results of the low-temperature neutron diffraction study of β-CD·11D_2O carried out by Zabel et al. (*9*). This work demonstrated that at the temperature of 120 K, all the existing flip-flop H-bonds had been transformed into those of normal type with the exception of a four-membered ring which consisted of flip-flop H-bonds and was positioned at the junction of several homodromic rings and infinite chains. The above phenomenon was attributed to an energetic advantage at 120 K over an entropy advantage at room temperature. Furthermore, Hanabata et al. (*51*) conducted a calorimetric study of β-CD·11H_2O and reported a first-order phase transition at 226 K along with a glass transition behaviour of the sample at ~ 150 K which was correlated with the frozen-in disorder of the proton configurations engaged in the four-membered ring. Finally, the dielectric investigation of β-CD·11H_2O by Pathmanathan et al. (*52*) exhibited apart from the order–disorder transition (*7*) at 209.8 K, a relaxation peak of the imaginary part ε'' at 109 K which was attributed to the occurrence of localised molecular motions in an otherwise rigid matrix. Thus, in the present case, the relaxation peak at 128.8 K comprises strong evidence for the formation of a flip-flop ring in the low temperature region despite the complete ordering (glass-like state) in the rest hydrogen-bonding network. The exact structural characteristics of such a ring can only be determined via a detailed single crystal neutron diffraction study of (α-CD)-Sr and for this reason we do not proceed to any further interpretation. However, the fact that (α-CD)-Sr presents similar behaviour to β-cyclodextrin undecahydrate and not to the (α-CD)-Cd and (α-CD)-Na complexes (single relaxation peaks at $T < 250$ K) (*4–6*) is a matter of concern.

Above the temperature of ~ 250 K, the conductance of (α-CD)-Sr increases enormously resulting in very high values of ε' and ε'' that have no significance in the conventional dielectric sense (*53*). Therefore, we turn our attention to the temperature dependence of the AC-conductivity σ which provides valuable information about all the different charge transport properties that appear in the range of 110–440 K. In the lnσ vs. 1/T plot (Figure 14), the broad bell-shaped curve (a) at 128.8 K corresponds to the frozen-in disorder in the hydrogen-bonding network, whereas the broad bell-shaped curve (b) at 173.7 K is caused by the order–disorder transition (*7*). The linear part (c) in the range of 254.5–329.4 K

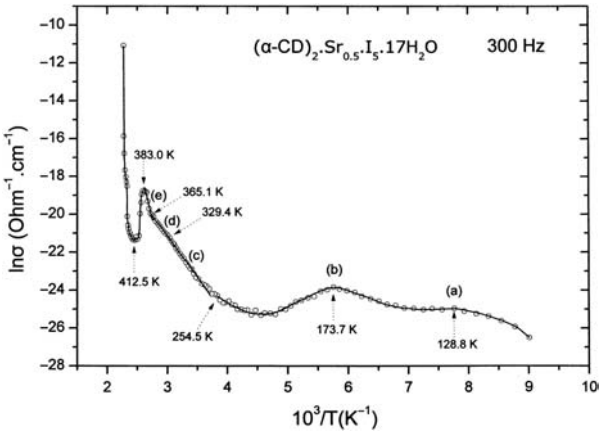

Figure 14. Temperature dependence of the AC-conductivity σ (lnσ *vs.* 1/T) of (α-CD)$_2$·$Sr_{0.5}$·I_5·17H_2O at 300 Hz.

exhibits an Arrhenius behaviour according to the semiconduction Equation (*54*, *55*):

$$\sigma = \sigma_o \exp\left[-\frac{E_a}{kT}\right], \tag{8}$$

where activation energy $E_a = 0.37$ eV, σ_o is the pre-exponential factor, k the Boltzmann's constant and T the absolute temperature. This exponential variation of the AC-conductivity is a consequence of the gradual transformation:

$$(H_2O)_{\text{tightly bound}} \rightarrow (H_2O)_{\text{easily movable}}, \tag{9}$$

which takes place along with the strontium ions' movements as it becomes evident from the impedance diagram of Figure 15. The appearance of the semicircular arcs reveals that the behaviour of the complex impedance Z^* in the present case can be described by the Cole–Cole

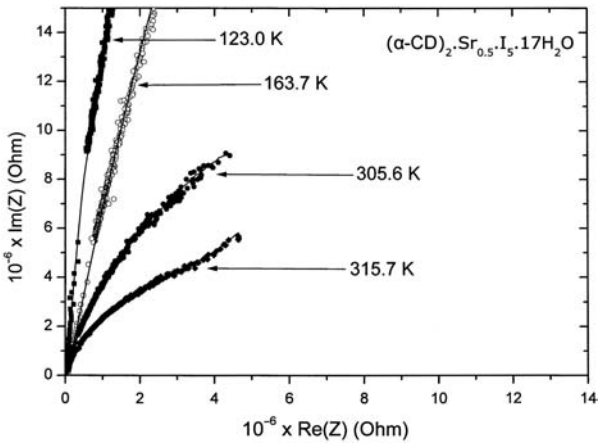

Figure 15. Impedance plot of (α-CD)$_2$·$Sr_{0.5}$·I_5·17H_2O at the representative temperatures of 123.0, 163.7, 305.6 and 315.7 K.

formalism (*56*, *57*):

$$Z^*(\omega) = \frac{Z_s - Z_\infty}{1 + (j\omega\tau)^{1-\alpha}}, \quad (10)$$

where Z_s is the static or the DC resistance R_{DC}, Z_∞ is the impedance at high frequency and α represents a measure of the distribution of relaxation times. During the heating process, the radii of the semicircular arcs decrease because the thermally activated processes (7) and (9) involve a continuous increment of the positionally disordered protons, H_2O molecules and OH-groups causing a progressive reduction in the grain interior resistance. Furthermore, the remarkably increased degree of disorder in the hydrogen-bonding network due to energy gain with temperature rise implies the cleavage of certain H-bond geometries and the initiation of a proton hopping process described as Grotthuss mechanism (*58–60*). The generation of the linear response in the low frequency region at $\sim$ 315.7 K is associated with the onset of space charge in the material (*61*, *62*), an effect which is directly related to the release of Sr^{2+} ions and their successive oscillations with the frequency of the applied alternative field. This diffusive process is so much slower than any other diffusive process in the crystal lattice (hydrogen bond dynamics occur in a timescale of $10^{-11} - 10^{-6}$ s (*43*, *59*, *63*)) and therefore it is responsible for the appearance of the aforementioned linear response.

The linear part (d) in the temperature range of 329.4–365.1 K also follows the semiconduction Equation (8) with $E_a = 0.34$ eV. This activation energy is slightly lower than that of the linear part (c) because the progressive dehydration process reduces the number of the reoriented H_2O dipoles (easily movable state) in the interstices (first endothermic peak in Figure 10). Surprisingly, the linear part (e) in the range of 365.1–383 K presents an activation energy with the very high value of 1.16 eV. This experimental feature reveals that there is a population of H_2O molecules which remains in the tightly bound state (fully occupied sites) as the temperature is raised, due to the existence of very strong intermolecular interactions in the corresponding local environments (this population is responsible for the endothermic shoulder shown in Figure 10). Above 365.1 K, these rigid hydrogen-bonding arrangements are perturbed resulting in a considerable mobility of the involved water molecules and an unexpected increasing rate of the AC-conductivity which does not seem to be essentially affected by the simultaneous dehydration in this temperature range. It is noteworthy that the enormous increase of σ up to 383 K is consistent with the abrupt decrease of φ up to the same temperature (Figure 13), revealing that the sample conductance is being dominated by the disorder phenomena in the hydrogen-bonding network. At $T > 383$ K, the AC-conductivity decreases rapidly due to the fact that the dehydration process starts to have a significant impact on the electrical properties leading to both the extensive breakdown of the water network and the attenuation of the proton conduction. Moreover, the continuous removal of the water molecules from the crystal lattice gradually minimises the contribution of the strontium ions that act as localised charges. The remarkable increment of the AC-conductivity at $T > 412.5$ K is caused by the sublimation of iodine which provides conduction paths along the polyiodide chains resulting in an enhanced connectivity between the neighbouring building blocks and important electron delocalisation (long-range Coulomb attraction of excited electron and hole) (*34*, *35*, *64*). This phenomenon is also responsible for the rapid drop of the phase shift φ at $T > 412.5$ K (Figure 13). The topical minimum value of φ (54.1°) at 403.5 K is attributed to the structural transition (I) → (III) which a certain number of pentaiodide units undergo. This transition is analytically described in Figure 1(d) and was originally detected in the case of (α-CD)-Cd (*5*).

4. Concluding remarks

Interestingly, at $T < 250$ K the dielectric behaviour of (α-CD)-Sr is similar to the one of β-CD undecahydrate and significantly different from that of the previously investigated α-CD polyiodide complexes with Cd^{2+} and Na^+ ions. The relaxation peak at 128.8 K indicates the persistence of localised proton motions (frozen-in disorder) in the glass-like state (complete ordering in the rest H-bonding network) of (α-CD)-Sr, whereas the relaxation peak at 173.7 K is consistent with the transition of some normal H-bonds to those of flip-flop type. At $T > 250$ K, the AC-conductivity σ increases abruptly due to the gradual transformation $(H_2O)_{\text{tightly bound}} \rightarrow (H_2O)_{\text{easily movable}}$ (also confirmed via DSC measurements) and the mobility of the released Sr^{2+} ions. Above 383 K, the AC-conductivity drops rapidly because the dehydration process starts to have an important impact on the electrical properties leading to both the extensive breakdown of the water network and the minimisation of metal ions' contribution. Furthermore, the enormous increment of the AC-conductivity at $T > 412.5$ K is attributed to the sublimation of iodine. Concerning the polyiodide moieties of (α-CD)-Sr, four discrete pentaiodide structural features were found to coexist at room temperature (298 K) depending on the occupancy ratio (x/y) of the central I^- ions. In the ($I_3^- \cdot I_2 \leftrightarrow I_2 \cdot I_3^-$) units (form (I)) $x/y \neq 50/50$ (e.g. ...60/40...70/30...). The ($I_2 \cdot I^- \cdot I_2$) units can be classified as the two equivalent forms (IIa) and (IIb). In (IIa) $x/y = 50/50$, whereas in (IIb) $x/y = 100/0$ (a ratio indicative of full occupancy). Finally, in the ($I_3^- \cdot I_2$) units (form (III)) the I^- ion is well ordered (100/0) forming with the one of the two I_2 molecules, a triiodide ion. As the crystals are slowly cooled, the transformation (I) → (IIa) takes place, whereas during the heating process the inverse transformation (IIa) → (I) occurs. These phenomena are caused by the changes in the corresponding occupancy ratios

(x/y) as the thermal variation of the sample proceeds. At 403.5 K, a certain number of I_5^- ions undergo the disorder–order transition (I) → (III). The initial (298 K) forms (IIb) and (III) remain unaffected by temperature.

Acknowledgement

The authors are grateful to the NKUA for partial financial support, Grant No. 70/4/3347SARG.

References

(1) Cramer, F.; Bergmann, U.; Manor, P.C.; Noltemeyer, M.; Saenger, W. *Justus Liebigs Ann. Chem.* **1976**, *7/8*, 1169–1179.
(2) Noltemeyer, M.; Saenger, W. *Nature* **1976**, *259*, 629–632.
(3) Noltemeyer, M.; Saenger, W. *J. Am. Chem. Soc.* **1980**, *102*, 2710–2722.
(4) Ghikas, T.C.; Papaioannou, J.C. *Mol. Phys.* **2002**, *100*, 673–679.
(5) Charalampopoulos, V.G.; Papaioannou, J.C.; Tampouris, K.E. *Solid State Ionics* **2007**, *178*, 793–799.
(6) Charalampopoulos, V.G.; Papaioannou, J.C. *Carbohydr. Res.* **2007**, *342*, 2075–2085.
(7) Saenger, W.; Betzel, Ch.; Hingerty, B.; Brown, G.M. *Nature* **1982**, *296*, 581–583.
(8) Betzel, Ch.; Saenger, W.; Hingerty, B.E.; Brown, G.M. *J. Am. Chem. Soc.* **1984**, *106*, 7545–7557.
(9) Zabel, V.; Saenger, W.; Mason, S.A. *J. Am. Chem. Soc.* **1986**, *108*, 3664–3673.
(10) Roux, B.; Karplus, M. *Annu. Rev. Biophys. Biomol. Struct.* **1994**, *23*, 731–761.
(11) Quigley, E.P.; Quigley, P.; Crumrine, D.S.; Cukierman, S. *Biophys. J.* **1999**, *77*, 2479–2491.
(12) Pomes, R.; Roux, B. *Biophys. J.* **2002**, *82*, 2304–2316.
(13) Bhattacharyya, K.; Bagchi, B. *J. Phys. Chem. A* **2000**, *104*, 10603–10613.
(14) Nandi, N.; Bhattacharyya, K.; Bagchi, B. *Chem. Rev.* **2000**, *100*, 2013–2046.
(15) Svensson, P.H.; Kloo, L. *Chem. Rev.* **2003**, *103*, 1649–1684.
(16) Haller, J.; Kaatze, U. *J. Mol. Liq.* **2008**, *138*, 34–39.
(17) Haller, J.; Kaatze, U. *J. Phys. Chem. B* **2009**, *113*, 1940–1947.
(18) Svensson, P.H.; Kloo, L. *J. Chem. Soc. Dalton Trans.* **2000**, 2449–2455.
(19) Kraus, W.; Nolze, G. *J. Appl. Crystallogr.* **1996**, *29*, 301–303.
(20) Nolze, G.; Kraus, W. *Powder Diffr.* **1998**, *13*, 256–259.
(21) Irsen, S.H.; Dronskowski, R. *Z. Naturforsch* **2002**, *57b*, 1387–1390.
(22) Isaenko, L.; Yelisseyev, A.; Lobanov, S.; Titov, A.; Petrov, V.; Zondy, J.J.; Krinitsin, P.; Merkulov, A.; Vedenyapin, V.; Smirnova, J. *Cryst. Res. Technol.* **2003**, *38*, 379–387.
(23) Efimov, V.V.; Efimova, E.A.; Iakoubovskii, K.; Kaprinskii, D.V.; Khasanov, S.; Kochubey, D.I.; Kriventsov, V.V.; Kuzmin, A.; Sazonov, A.P.; Sikolenko, V.; Sakharov, M.; Shmakov, A.N.; Tiutiunnikov, S.I. *J. Phys. Chem. Solids* **2006**, *67*, 2001–2006.
(24) Papaioannou, J.C.; Papadimitropoulos, N.; Mavridis, I. *Mol. Phys.* **1999**, *97*, 611–627.
(25) Charalampopoulos, V.G.; Papaioannou, J.C. *Mol. Phys.* **2005**, *103*, 2621–2631.
(26) Teitelbaum, R.C.; Ruby, S.L.; Marks, T.J. *J. Am. Chem. Soc.* **1980**, *102*, 3322–3328.
(27) Nour, E.M.; Chen, L.H.; Laane, J. *J. Phys. Chem.* **1986**, *90*, 2841–2846.
(28) Mizuno, M.; Tanaka, J.; Harada, I. *J. Phys. Chem.* **1981**, *85*, 1789–1794.
(29) Mittag, H.; Stegemann, H.; Füllbier, H.; Irmer, G. *J. Raman Spectrosc.* **1989**, *20*, 251–255.
(30) Yu, X.; Houtman, C.; Atalla, R.H. *Carbohydr. Res.* **1996**, *292*, 129–141.
(31) Yu, X.; Atalla, R.H. *Carbohydr. Res.* **2005**, *340*, 981–988.
(32) Deplano, P.; Devillanova, F.A.; Ferraro, J.R.; Mercuri, M.L.; Lippolis, V.; Trogu, E.F. *Appl. Spectrosc.* **1994**, *48*, 1236–1241.
(33) Deplano, P.; Ferraro, J.R.; Mercuri, M.L.; Trogu, E.F. *Coord. Chem. Rev.* **1999**, *188*, 71–95.
(34) Sengupta, A.; Quitevis, E.L.; Holtz, M.W. *J. Phys. Chem. B* **1997**, *101*, 11092–11098.
(35) Mulazzi, E.; Pollini, I.; Piseri, L.; Tubino, R. *Phys. Rev. B* **1981**, *24*, 3555–3653.
(36) Dunitz, J.D.; Schomaker, V.; Trueblood, K.N. *J. Phys. Chem.* **1988**, *92*, 856–867.
(37) Brock, C.P.; Morelan, G.L. *J. Phys. Chem.* **1986**, *90*, 5631–5640.
(38) Bürgi, H.B. *Ann. Rev. Phys. Chem.* **2000**, *51*, 275–296.
(39) Wilson, C.C. *Crystallogr. Rev.* **2009**, *15*, 3–56.
(40) Muetterties, E.L. *Inorg. Chem.* **1965**, *4*, 769–771.
(41) Anderson, A.; Sun, T.S. *Chem. Phys. Lett.* **1970**, *6*, 611–616.
(42) Sharp, S.B.; Gellene, G.I. *J. Phys. Chem. A* **1997**, *101*, 2192–2197.
(43) Steiner, Th.; Koellner, G. *J. Am. Chem. Soc.* **1994**, *116*, 5122–5128.
(44) Bettinetti, G.; Novak, Cs.; Sorrenti, M. *J. Thermal Anal. Calorim.* **2002**, *68*, 517–529.
(45) Charalampopoulos, V.G.; Papaioannou, J.C.; Karayianni, H.S. *Solid State Sci.* **2006**, *8*, 97–103.
(46) Papaioannou, J.C.; Charalampopoulos, V.G.; Xynogalas, P.; Viras, K. *J. Phys. Chem. Solids* **2006**, *67*, 1379–1386.
(47) Charalampopoulos, V.G.; Papaioannou, J.C. *Solid State Ionics* **2008**, *179*, 565–573.
(48) Liu, J.; Duan, C.-G.; Yin, W.-G.; Mei, W.N.; Smith, R.W.; Hardy, J.R. *Phys. Rev. B* **2004**, *70*, 144106–144112.
(49) Ahmad, M.M.; Yamada, K.; Okuda, T. *Solid State Commun.* **2002**, *123*, 185–189.
(50) Macdonald, J.R. *Impedance Spectroscopy*; Wiley: New York, 1987; p 1.
(51) Hanabata, H.; Matsuo, T.; Suga, H. *J. Inclusion Phenom.* **1987**, *5*, 325–333.
(52) Pathmanathan, K.; Johari, G.P.; Ripmeester, J.A. *J. Phys. Chem.* **1989**, *93*, 7491–7494.
(53) West, A.R. *Solid State Chemistry and its Applications*; Wiley: New York, 1984; p 535.
(54) Kidner, N.J.; Meier, A.; Homrighaus, Z.J.; Wessels, B.W.; Mason, T.O.; Garboczi, E.J. *Thin Solid Films* **2007**, *515*, 4588–4595.
(55) Dutta, A.; Sinha, T.P. *J. Phys. Chem. Solids* **2006**, *67*, 1484–1491.
(56) Sen, S.; Pramanik, P.; Choudhary, R.N.P. *Appl. Phys. A Mater. Sci. Process* **2006**, *82*, 549–557.
(57) Macdonald, J.R. *Impedance Spectroscopy*; Wiley: New York, 1987; p 27.
(58) de Grotthuss, C.J.T. *Ann. Chim.* **1806**, *58*, 54–74.
(59) Agmon, N. *Chem. Phys. Lett.* **1995**, *244*, 456–462.
(60) Merinov, B.V. *Solid State Ionics* **1996**, *84*, 89–96.
(61) Jonscher, A.K. *J. Mater. Sci.* **1978**, *13*, 553–562.
(62) Macdonald, J.R. *Impedance Spectroscopy*; Wiley: New York, 1987; p 252.
(63) Steiner, Th.; Saenger, W.; Lechner, R.E. *Mol. Phys.* **1991**, *72*, 1211–1232.
(64) Oza, A. *Cryst. Res. Technol.* **1984**, *19*, 697–707.